Wideband Microstrip Coupled-Line Ring Hybrids for High Power-Division Ratios

Hee-Ran Ahn, *Senior Member, IEEE*, and Sangwook Nam, *Senior Member, IEEE*

***Abstract*—Wideband coupled-line ring hybrids are presented for high power-division ratios. For this, an equivalent circuit to make the characteristic impedance of a transmission-line section lower is firstly investigated, based on a Π-type lumped-element equivalent circuits. Design formulas of four types of equivalent circuits (L_Π-, L_T-, L_{S2}-, and L_{S1}-types) are then derived, and N is introduced for more design flexibility and wideband performance. The L_{S2}-type with $N = 1$ is composed of one transmission-line section and two identical series inductances at both ends, which cannot be used for the ring hybrids with the high power-division ratios. To avoid the problem, modified L_{S2}-type (ML_{S2}-type) with N is additionally suggested, and that with $N = 1$ is intensively discussed. Using two of those, L_{S1}-type with $N = 2$ and ML_{S2}-type with $N = 1$, the coupled-line ring hybrids with 13- and 11-dB power-division ratios are fabricated. The measured results show good agreement with those predicted.**

***Index Terms*—Arbitrary power divisions, coupled-line ring hybrids with high power-division ratios, coupled transmission-line sections with very high characteristic impedances, equivalent circuits of high-impedance transmission-line sections, high-impedance transmission-line sections, rat-race couplers with arbitrary power divisions.**

I. Introduction

THE RING hybrids [1]–[11] consist of three 90° and one 270° transmission-line sections, the 270° section of which may be replaced with a set of 90° coupled transmission-line sections for wideband performance [2], [3], [11]. The ring hybrids have been used for various applications, such as phase shifters [12], antenna arrays, mixers, and balancing amplifiers, and for those applications, arbitrary power divisions are needed. In this case, if the power-division ratios are very high, i.e., more than 9 dB, the transmission-line sections with the characteristic impedances higher than 150 Ω are indispensible [2], [5]–[9] under the assumption of 50-Ω termination impedances. The characteristic impedances higher than 150 Ω are, however, not easy to implement with microstrip formats, and therefore, the restriction on the fabrication [6] with such high power-division ratios may be inevitable. There have been previous publications treating arbitrary power divisions [2], [5]–[10] and are compared in Table I, in terms of power-division ratios ($P_{\rm dB}$). For comparisons, if the bandwidths are not specified, they were simulated based on design data given in the papers, and the bandwidths were extracted on the basis of the simulation results.

TABLE I
Comparisons in Terms of Power-Division Ratios

Refs	Bandwidths ($P_{\rm dB} \pm 0.5$dB)	$P_{\rm dB}$	Fabrication
[2]	≥ 180%	4 dB	uniplanar
[5]	≈ 23.6 %	3.98 dB	microstrip
[6]	≈ 21.2 %	11.3 dB	microstrip
[7]	≈ 2-3%	6 dB	microstrip
[8]	≈ 9.0 %	9 dB	microstrip
[9]	less than 10%	6 dB	microstrip
[10]	≈ 22.2%	6 dB	microstrip
This work	≈ 108%	13 dB	microstrip

The bandwidth [2] is greater than 180% due to a 180° phase shifter of coplanar strip twist, but $P_{\rm dB}$ is 4 dB. The typical ring hybrid in [5] has the bandwidth of 23.6%, while that of the modified structure in [6] is 21.2% where $P_{\rm dB} = 11.3$ dB is measured in [6], but perfect matching does not appear. In addition, several others in [7]–[10] are available, but the bandwidths are smaller since the two [7], [9] are reduced, and the one in [8] is designed to achieve the desired power divisions only at the design center frequency. The design in [10] may start from one ring hybrid consisting of two 270° and two arbitrary lengths of transmission-line sections, and two 270° transmission-line sections are simplified as two variable capacitors to control the power divisions. Therefore, the bandwidth is not small even with smaller size. The ring hybrids in this paper are fabricated for $P_{\rm dB} = 11$ and 13 dB, and $P_{\rm dB} = 13$ dB is compared. In this case, the bandwidth is 108%.

The ring hybrid to be treated in this paper consists of one set of coupled transmission-line sections and are therefore called the coupled-line ring hybrid [3]. The coupled-line sections [2], [3] have inherently a 180° phase shifter, and thus the 180° phase difference between 90° coupled-line sections and single transmission-line sections can be achieved in much wider range of frequencies than between 90° and 270° single transmission-line sections, which is already demonstrated in [3, Fig. 2]. That is, the coupled-line ring hybrid consisting of three 90° sections and one 90° coupled-line sections has much wider bandwidths than a conventional ring hybrid.

The coupled-line sections are, for the first time, applied for the ring hybrids by March [11], but the application is valid

Manuscript received November 05, 2012; revised February 21, 2013; accepted February 23, 2013. Date of publication March 29, 2013; date of current version May 02, 2013. This work was supported by the Korea Communications Commission (KCC) under the Research and Development Program supervised by the Korea Communications Agency (KCA) [KCA-2012-(12-911-01-102)].

The authors are with the Institute of New Media and Communication (INMC), School of Electrical Engineering and Computer Science, Seoul National University, Seoul 151-742, Korea (e-mail: hranahn@gmail.com; snam@snu.ac.kr).

Color versions of one or more of the figures in this paper are available online at http://ieeexplore.ieee.org.

Digital Object Identifier 10.1109/TMTT.2013.2251654

only and only if the coupling coefficient is -3 dB. To employ the coupled-line sections with no restriction on the coupling coefficients, new design formulas are derived [3], and high-impedance transmission-line sections generated by them are treated [13]. The reason for the bandwidth of 108% in Table I even with the 180° phase shifter is because of the coupling coefficient of -8.5 dB.

The 180° phase shifters may be obtained from a coplanar waveguide (CPW) inverter [14, Fig. 7(a)], CPW-slot line transitions [4, Fig. 3.23(d) and (e)] and [15, Fig. 9], and coplanar strip twist [2, Fig. 7]. They are, however, not microstrip lines and require air-bridges, for which careful implementation is demanded.

For the high power-division ratios, one single and one set of coupled transmission-line sections with high values of the characteristic impedances are necessary. To make a single transmission-line section with high characteristic impedances feasible, four types of equivalent circuits are discussed, and an integer N is introduced. The unit element of the first type is named L_{Π}-type, which is composed of one transmission-line section and two identical shunt inductances, being connected at both ends of the transmission-line section. The second one is designated as L_T-type, which consists of two identical transmission-line sections and one shunt inductance, being connected at the center of the two transmission-line sections. The third one is called L_{S2}-type, being made of one transmission-line section and two inductances, which are connected in series to both ends of the transmission-line section. The fourth is denominated L_{S1}-type, which is comprised of two identical transmission-line sections and one inductance, connected at the center of the two transmission-line sections in series. The equivalent circuits proposed in this paper are those with N's unit elements connected in cascade for wideband performance and design flexibility. For the coupled-line sections, the design formulas in [3], [13], [16], and [17] are adopted.

In the conventional designs, L_T- [18] and L_{S2}-types [19] are suggested, but both are confined to the narrow bandwidth with $N = 1$. Furthermore, the L_{S2}-type [19] cannot be applied for the ring hybrid with the high power-division ratios, due to two inductors located at both ends, even though the characteristic impedances of the transmission-line section in the L_{S2}-type may be lower than that of an original transmission-line section. Therefore, the application in [19] is limited to the characteristic impedances of 35.35 to 50 Ω, the operating frequencies more than 20 GHz and monolithic microwave integrated circuit (MMIC) (CPW) technology.

The two inductances of the L_{S2}-type are located at both sides, each value of which is inversely proportional to the operating frequency, but proportional to the characteristic impedances of the original transmission-line section. If operating frequencies are less than 5 GHz and the characteristic impedances of the original transmission line sections are higher than 180 Ω, the inductance values are so high that they should be realized with lumped-element inductors. In this case, since a 50-Ω transmission-line section can be wider than two times the lengths of a lumped inductor, it is almost impossible to correctly fabricate the L_{S2}-type with microstrip technology, due to the difficulty in making a Y-junction, i.e., producing a port or connecting another transmission-line section or diodes. To make the single transmission-line section feasible with the similar L_{S2}-type, modified L_{S2}-type (ML_{S2}-type) is suggested. The ML_{S2}-type has one L_{S2}-type and two additional identical transmission-line sections connected at both ends of the L_{S2}-type. Since the two transmission-line sections of the ML_{S2}-type can be chosen arbitrarily, design flexibility may be improved. To fulfill engineering perspective that the simplest is generally the most preferable, the ML_{S2}-type with $N = 1$ is intensively discussed and compared with L_{S2}-types with $N = 1$ and 2. The compared results show that the frequency performance of the ML_{S2}-type with $N = 1$ is better than the L_{S2}-type with $N = 2$, even with less number of inductances.

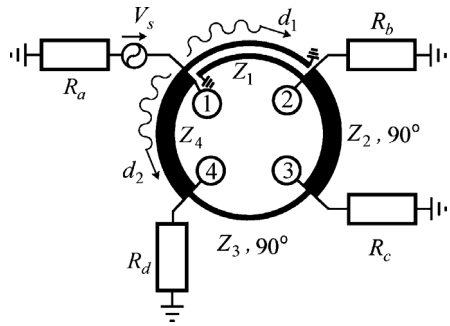

Fig. 1. Coupled-line ring hybrid with arbitrary termination impedances of R_a, R_b, R_c, and R_d.

High-impedance transmission-line sections [20]–[22] were treated, in addition to the conventional L_T-type [18], but they require more process steps to design and etch ground planes, being unsuitable for pure microstrip technology. Moreover, all the applications by the conventional methods [16]–[18], [20]–[22] are not for the ring hybrids.

To verify the suggested theory, two microstrip coupled-line ring hybrids with the power-division ratios of 13 and 11 dB are fabricated, and the measured results show good agreement with those predicted.

II. Coupled-Line Ring Hybrids

The coupled-line ring hybrid for arbitrary power-division ratios is depicted in Fig. 1 where it is terminated in arbitrary real impedances of R_a, R_b, R_c, and R_d at ports ①, ②, ③, and ④. The ring hybrid consists of three 90° transmission-line sections and one set of 90° coupled transmission-line sections terminated in two short circuits in a diagonal direction. The effective characteristic impedance of the coupled transmission-line sections is Z_1, while those of the three single sections are Z_2, Z_3, and Z_4.

If the scattering parameter ratio of $|S_{41}|/|S_{21}|$ is d_2/d_1, as indicated in Fig. 1, the design equations for Z_1, Z_2, Z_3, and Z_4 [2] are

$$Z_1 = \sqrt{1 + 10^{\frac{P_{\mathrm{dB}}}{10}}}\sqrt{R_a R_b} \tag{1a}$$

$$Z_2 = \sqrt{\frac{1 + 10^{\frac{P_{\mathrm{dB}}}{10}}}{10^{\frac{P_{\mathrm{dB}}}{10}}}}\sqrt{R_b R_c} \tag{1b}$$

$$Z_3 = \sqrt{1 + 10^{\frac{P_{\mathrm{dB}}}{10}}}\sqrt{R_c R_d} \tag{1c}$$

TABLE II
CHARACTERISTIC IMPEDANCES WITH DIFFERENT $P_{\rm dB}$ UNDER THE ASSUMPTION OF EQUAL TERMINATION IMPEDANCES OF 50 Ω

$P_{\rm dB}$	$Z_1 = Z_3$ (Ω)	$Z_2 = Z_4$ (Ω)
9 dB	149.53 Ω	53.05 Ω
10 dB	165.83 Ω	52.44 Ω
11 dB	184.32 Ω	51.95 Ω
12 dB	205.24 Ω	51.56 Ω
13 dB	228.87 Ω	51.24 Ω

$$Z_4 = \sqrt{\frac{1+10^{\frac{P_{\rm dB}}{10}}}{10^{\frac{P_{\rm dB}}{10}}}\sqrt{R_a R_d}} \tag{1d}$$

where $P_{\rm dB}$ is the power-division ratio in dB and expressed as $20\log^{d_2/d_1}$.

$R_a = R_b = R_c = R_d = 50\ \Omega$ being assumed, the characteristic impedances of Z_1, Z_2, Z_3, and Z_4 are calculated by varying $P_{\rm dB}$ and listed in Table II. The characteristic impedances of Z_1 and Z_3 are proportional to the power-division ratios. To implement the ring hybrids with $P_{\rm dB} \geq 9$ dB, 90° transmission-line sections, which cannot be easily realized in microstrip technology, are indispensible as computed in Table II. The way to realize such transmission-line sections with the characteristic impedances higher than 150 Ω will be discussed in terms of single and coupled transmission-line sections.

III. SINGLE TRANSMISSION-LINE SECTIONS

In the case that the characteristic impedance of a single transmission-line section is too high to realize with the microstrip format, ways to make such high-impedance transmission-line sections feasible will be introduced in terms of a Π-type lumped-element equivalent circuit. Design formulas for the transmission-line section will then be derived based on the lumped-element approach.

A. Lumped-Element Approach

A Π-type lumped-element equivalent circuit of a transmission-line section with the characteristic impedance of Z_0 and the electrical length of Θ_u is depicted in Fig. 2 where the Π-type consists of two identical shunt capacitances of C_0 and one series inductance of L_0. Since the image impedance of the Π-type is equal to the characteristic impedance of the transmission-line section, Z_0 and Θ_u may be expressed with the lumped elements [4] such as

$$Y_0 = \sqrt{\omega C_0\left(\frac{2}{\omega L_0} - \omega C_0\right)} \tag{2a}$$

$$\cos\Theta_u = 1 - \omega^2 C_0 L_0 \tag{2b}$$

where $Y_0 = Z_0^{-1}$.

The characteristic impedances of Z_0 were calculated by fixing ωL_0 at 128.6 Ω and varying ωC_0, and the calculation results are plotted in Fig. 2 where the characteristic impedances are proportional to $(\omega C_0)^{-1}$, and $(\omega C_0)^{-1} = 549.5\ \Omega$ is needed for $Z_0 = 200\ \Omega$, as indicated in Fig. 2. If the characteristic impedance of an original transmission-line section is too high to fabricate, the lower value of Z_0 may be obtained by decreasing $(\omega C_0)^{-1}$ in the Π-type, keeping the characteristics

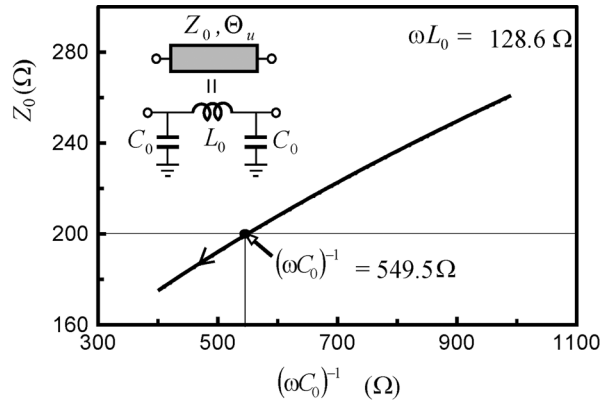

Fig. 2. Π-type equivalent circuit and its characteristic impedance variation.

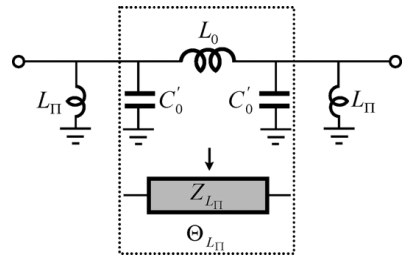

Fig. 3. Π-type lumped-element equivalent circuit with inductances added.

the same as those of the original transmission-line section. A way to increase ωC_0 for the Π-type is adding inductances to the original circuit.

A lumped-element circuit is described in Fig. 3, consisting of one series inductance of L_0 and two parallel resonators with each having an inductance of L_Π and a capacitance of C_0'. An inductance of L_0 and two identical capacitances of C_0' form another Π-type circuit, which can be equivalent to a transmission-line section with the characteristic impedance of Z_{L_Π} and the electrical length of Θ_{L_Π} assumed. If the lumped-element circuit in Fig. 3 is the same as that of the Π-type in Fig. 2, the capacitance of C_0' is

$$\omega C_0' = \omega C_0 + \frac{1}{\omega L_\Pi}. \tag{3}$$

The characteristic impedances of Z_{L_Π} and the electrical length of Θ_{L_Π} were calculated by varying the inductances of L_Π to see how much to deviate from the original transmission-line section. The calculation results are plotted in Fig. 4 where ωL_0 is fixed at $Z_0 \sin\Theta_u$, where $Z_0 = Y_0^{-1} = 200\ \Omega$ and $\Theta_u = 40°$, which means that the characteristic impedance and the electrical length of the original transmission-line section are $Z_0 = 200\ \Omega$ and $\Theta_u = 40°$.

In Fig. 4, the characteristic impedance of Z_{L_Π} has a minimum value of 128.5 Ω when L_Π is around 28 nH and close to 200 Ω when L_Π is close to infinite. The electrical length of Θ_{L_Π} is inversely proportional to the inductance of L_Π and approaches to 40°, when L_Π has a very large value. In other words, with no inductance of L_Π added, the characteristic impedance of Z_{L_Π} and the electrical length of Θ_{L_Π} becomes the same as those of the original one. Fig. 4 results from the calculation, and it

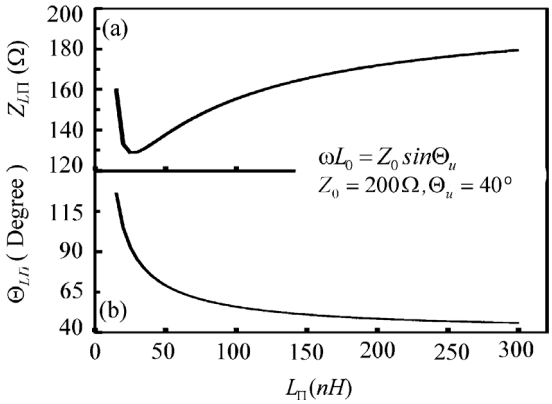

Fig. 4. Calculation results of characteristic impedance of Z_{L_Π} and electrical length of Θ_{L_Π}.

is found that a lower characteristic impedances of Z_{L_Π} can be obtained by adding less value of L_Π and that the electrical length of Θ_{L_Π} increases inversely with L_Π.

With this concept, three more equivalent circuits, by which the characteristic impedances of transmission-line sections can be lowered, may be derived using T-type and halves of Π- and T-types (L-sections) of the lumped-element equivalent circuits.

B. Design Formulas

A transmission-line section with the characteristic impedance of Z_0 and the electrical length of Θ/N is depicted in Fig. 5(a), and its four types of equivalent circuits are detailed in Fig. 5(b)–(d). The characteristic impedances of the transmission-line sections in the equivalent circuits in Fig. 5(b)–(d) are intended to be lower than Z_0 of the original transmission-line section, and N in Fig. 5(a) is a positive integer. To distinguish from each other, the four equivalent circuits are called L_Π-, L_T-, L_{S2}-, and L_{S1}-types. The L_Π-type in Fig. 5(b) consists of one transmission-line section with the characteristic impedance of Z_{L_Π} and the electrical length of Θ_{L_Π}, and two identical shunt inductances of L_Π, as demonstrated in Figs. 3 and 5(b). The L_T-type in Fig. 5(c) comprises two identical transmission-line sections with the characteristic impedance of Z_{L_T} and the electrical length of $\Theta_{L_T}/2$, and one shunt inductance of L_T. The L_{S2}-type in Fig. 5(d) is composed of one transmission-line section with the characteristic impedance of $Z_{L_{S2}}$ and the electrical length of $\Theta_{L_{S2}}$, and two identical series inductances of L_{S2}. The L_{S1}-type in Fig. 5(e) includes two identical transmission-line sections with the characteristic impedance of $Z_{L_{S1}}$ and the electrical length of $\Theta_{L_{S1}}/2$, and a series inductance of L_{S1}. If the characteristic impedances of Z_{L_Π}, Z_{L_T}, $Z_{L_{S2}}$, and $Z_{L_{S1}}$ in Fig. 5(b)–(d) are lower than that of the original transmission-line section, the four circuits in Fig. 5 are good candidates for the coupled-line ring hybrid with high power-division ratios. The design formulas will be derived using even- and odd-mode excitation analyses.

The even- and odd-mode impedances Z_{OC} and Z_{SC} of the transmission-line section in Fig. 5(a) are

$$Z_{OC} = -jZ_0 \cot\frac{\Theta}{2N} \tag{4a}$$

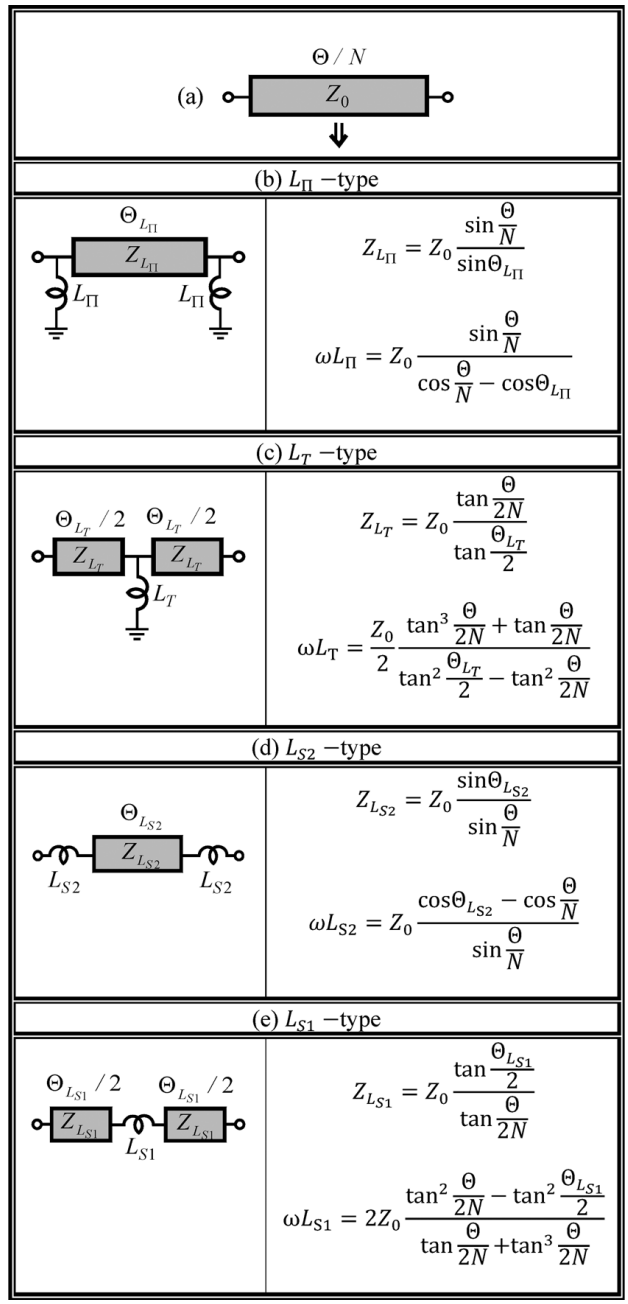

Fig. 5. Equivalent circuits. (a) Transmission-line section with Θ/N. (b) L_Π-type. (c) L_T-type. (d) L_{S2}-type. (e) L_{S1}-type.

$$Z_{SC} = jZ_0 \tan\frac{\Theta}{2N}. \tag{4b}$$

For the L_Π-type in Fig. 5(b), the even- and odd-mode admittances, $Y_{e\_L_\Pi}$ and $Y_{o\_L_\Pi}$ are

$$Y_{e\_L_\Pi} = \frac{1}{j\omega L_\Pi} + jY_{L_\Pi} \tan\frac{\Theta_{L_\Pi}}{2} \tag{5a}$$

$$Y_{o\_L_\Pi} = \frac{1}{j\omega L_\Pi} - jY_{L_\Pi} \cot\frac{\Theta_{L_\Pi}}{2} \tag{5b}$$

where $Y_{L_\Pi} = Z_{L_\Pi}^{-1}$.

For the L_T-type in Fig. 5(c), the even- and odd-mode impedances, $Z_{e\_L_T}$ and $Z_{o\_L_T}$ are

$$Z_{e\_L_T} = jZ_{L_T}\frac{2\omega L_T + Z_{L_T}\tan\frac{\Theta_{L_T}}{2}}{Z_{L_T} - 2\omega L_T\tan\frac{\Theta_{L_T}}{2}} \tag{6a}$$

$$Z_{o\_L_T} = jZ_{L_T}\tan\frac{\Theta_{L_T}}{2}. \tag{6b}$$

For the L_{S2}-type in Fig. 5(d), the even- and odd-mode impedances $Z_{e\_L_{S2}}$ and $Z_{o\_L_{S2}}$ are

$$Z_{e\_L_{S2}} = j\omega L_{S2} - jZ_{L_{S2}}\cot\frac{\Theta_{L_{S2}}}{2} \tag{7a}$$

$$Z_{o\_L_{S2}} = j\omega L_{S2} + jZ_{L_{S2}}\tan\frac{\Theta_{L_{S2}}}{2}. \tag{7b}$$

For the L_{S1}-type in Fig. 5(e), the even- and odd-mode impedances $Z_{e\_L_{S1}}$ and $Z_{o\_L_{S1}}$ are

$$Z_{e\_L_{S1}} = -jZ_{L_{S1}}\cot\frac{\Theta_{L_{S1}}}{2} \tag{8a}$$

$$Z_{o\_L_{S1}} = jZ_{L_{S1}}\frac{\frac{\omega L_{S1}}{2} + Z_{L_{S1}}\tan\frac{\Theta_{L_{S1}}}{2}}{Z_{L_{S1}} - \frac{\omega L_{S1}}{2}\tan\frac{\Theta_{L_{S1}}}{2}}. \tag{8b}$$

The design equations for the circuits in Fig. 5(b)–(e) are obtained by equating the even- and odd-mode impedances of the transmission-line section in (4) to each of those in (5)–(8) and summarized in Fig. 5 where $\Theta = 90°$ with $N = 1$ is excluded for the L_Π-type because Z_{L_Π} is greater than Z_0 with any value of Θ_{L_Π} for $\Theta = 90°$. To have the characteristic impedances of Z_{L_Π}, Z_{L_T}, $Z_{L_{S2}}$, and $Z_{L_{S1}}$ lower than Z_0, Θ_{L_Π} and Θ_{L_T} should be longer, whereas $\Theta_{L_{S2}}$ and $\Theta_{L_{S1}}$ should be shorter than Θ/N. Finally, the equivalent circuits for the electrical length of Θ of the transmission-line section are depicted in Fig. 6.

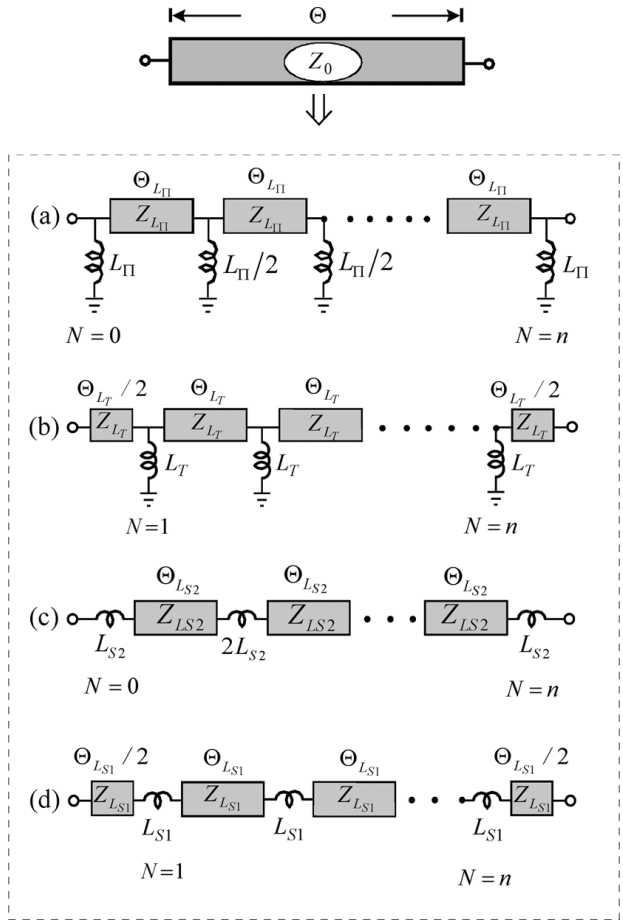

Fig. 6. Final equivalent circuits of a transmission-line section with Z_0 and Θ. (a) L_Π-type. (b) L_T-type. (c) L_{S2}-type. (d) L_{S1}-type.

C. Characteristic Impedances and Frequency Responses

a) L_Π- and L_T-Types: Based on the design equations in Fig. 5(b) and (c), the characteristic impedances of Z_{L_Π} and Z_{L_T} were calculated by varying N. The calculation results are listed in Table III and plotted in Fig. 7. In this case, the characteristic impedance and electrical length of the original transmission-line section are $Z_0 = 180\ \Omega$ and $\Theta = 90°$.

The resulting characteristic impedances of Z_{L_Π} and Z_{L_T} in Fig. 6 are, in any case, smaller than or equal to 180 Ω and inversely proportional to the total electrical length of $N\Theta_{L_\Pi}$ or $N\Theta_{L_T}$. If it is assumed that a characteristic impedance of 120 Ω may be realized without any difficulty, when $N = 5$ in Fig. 7(a), $N\Theta_{L_\Pi} = 138°$ is needed for the L_Π-type, while $N\Theta_{L_T} = 133.6°$ for the L_T-type. When $N = 2$ in Fig. 7(d), the required electrical length for the characteristic impedance of 120 Ω is $N\Theta_{L_T} = 127.4°$ for the L_T-type, but no solution exists for the L_Π-type. With increasing N, the difference between Z_{L_Π} and Z_{L_T} becomes smaller, and the two values are about the same when $N = 5$ in Fig. 7(a).

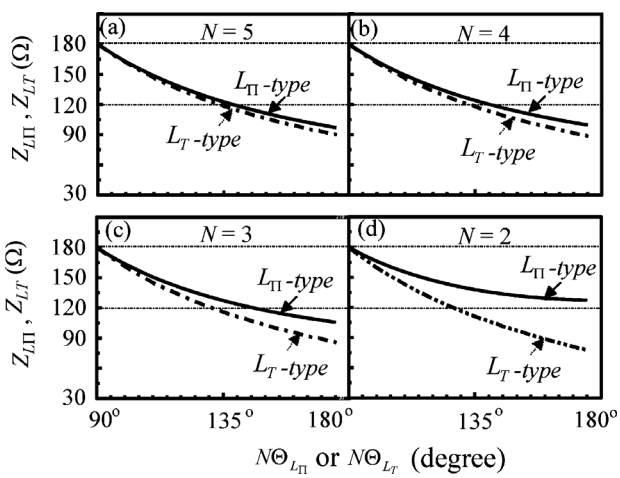

Fig. 7. Characteristic impedances of Z_{L_Π} and Z_{L_T} for a transmission-line section with $Z_0 = 180\ \Omega$ and $\Theta = 90°$. (a) $N = 5$. (b)$N = 4$. (c) $N = 3$. (d)$N = 2$.

The L_Π- and L_T-types with $N = 2$ and 1 were designed at a design center frequency of 1 GHz, and frequency responses of $|S_{11}|$ are compared in Fig. 8 where solid lines are those with $N = 2$, and the dotted line is that with $N = 1$ [18]. In this case, the characteristic impedance and the electrical length of the original transmission-line section are $Z_0 = 180\ \Omega$ and $\Theta = 90°$, and $N\Theta_{L_\Pi} = N\Theta_{L_T} = 135°$ was chosen for the simulations. If a bandwidth is defined as a frequency range where return loss is greater than 15 dB, the bandwidths of the L_Π- and L_T-types with $N = 2$ are 81% (0.9–1.71 GHz) and

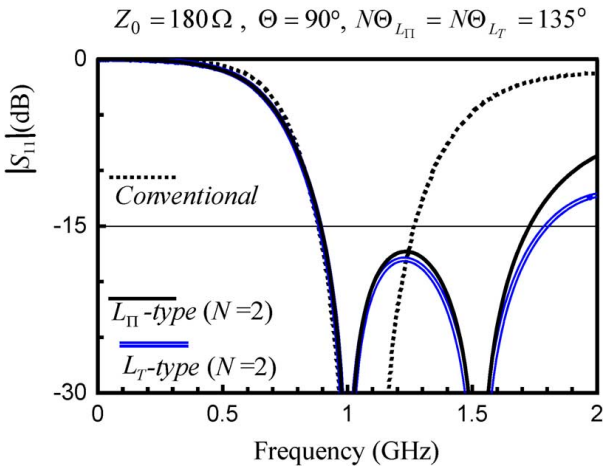

Fig. 8. Comparisons between the conventional (L_T-type with $N = 1$), L_Π- and L_T-types with $N = 2$.

TABLE III
DESIGN DATA OF L_Π- AND L_T-TYPES OF EQUIVALENT CIRCUITS WITH $Z_0 = 180\ \Omega$ AND $\Theta = 90°$

	$N\Theta_{L_\Pi} = N\Theta_{L_T} = 135°$		$N\Theta_{L_\Pi} = N\Theta_{L_T} = 120°$	
N	Z_{L_Π} (Ω)	Z_{L_T} (Ω)	Z_{L_Π} (Ω)	Z_{L_T} (Ω)
$N = 2$	137.77	111.59	146.97	129.14
$N = 3$	127.28	116.44	140.02	132.51
$N = 4$	123.99	118.03	137.77	133.62
$N = 5$	122.52	118.75	136.76	134.13

90% (0.9–1.8 GHz), respectively, while that with $N = 1$ is only 36% (0.9–1.26 GHz). The reason for the wider bandwidths with $N = 2$ is because of another resonance frequency made by increasing the number of N.

Based on the data in Table III, frequency responses of L_Π- and L_T-types are plotted in Fig. 9 where $N\Theta_{L_\Pi} = N\Theta_{L_T} = 135°$ is fixed and the number of N is varied. All the cases in Fig. 9 are perfectly matched at the design center frequency of 1 GHz, and several other matching frequencies exist. Independent of N, the second matching frequency is around 1.53 GHz, and the second frequency with 15-dB return loss is around 1.79 GHz. With N growing, the frequency responses of both equivalent circuits are about the same, but the optimum number of N is 2 for this case.

b) Measurements of L_T-Type With $N = 2$: To verify the L_T-type with $N = 2$, one with $Z_0 = 180\ \Omega$ and $\Theta = 90°$ was designed at a design center frequency of 2 GHz and fabricated on a substrate (RT/Duroid 5880, $\varepsilon_r = 2.2$, $H = 0.787$ mm). If $N = 2$ is chosen, Z_{L_T} in Fig. 6(b) becomes 111.59 Ω with $N\Theta_{L_T} = 135°$, which can be realized without any problem. The inductance of L_T is implemented with a short stub with the characteristic impedance of 120 Ω. The fabricated L_T-type is displayed in Fig. 10. Since the circuit in Fig. 10 is terminated in 180 Ω, there is no way to directly measure it. After measuring the circuit with the termination impedances of 50 Ω, the measured data are transformed into those with 180-Ω termination impedances using Agilent's Advanced Design System (ADS). The results measured and predicted are compared in Fig. 11 where quite good agreement between the two types of results is obtained.

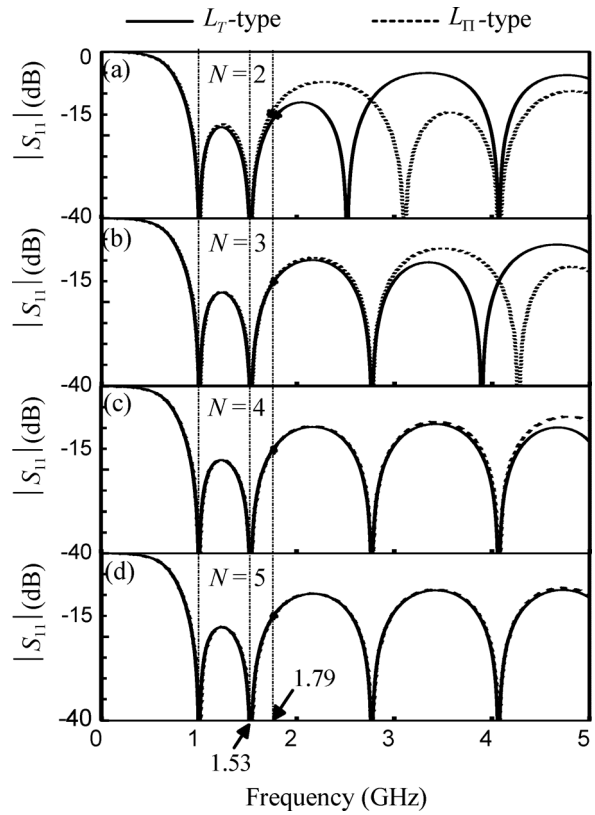

Fig. 9. Frequency responses of L_Π- and L_T-types. (a) $N = 2$. (b)$N = 3$. (c) $N = 4$. (d) $N = 5$.

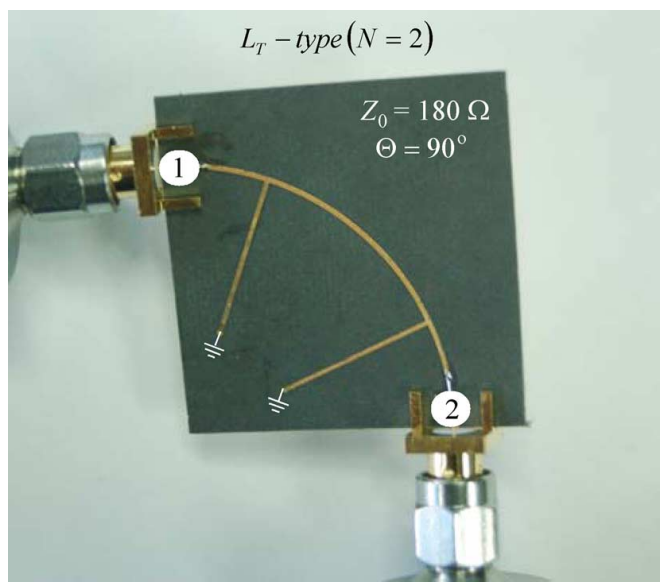

Fig. 10. Photograph of a L_T-type with $Z_0 = 180\ \Omega$ and $\Theta = 90°$.

c) L_{S2}- and L_{S1}-Types: Based on the design equations in Fig. 5(d) and (e), the characteristic impedances of $Z_{L_{S2}}$ and $Z_{L_{S1}}$ for $Z_0 = 180\ \Omega$ and $\Theta = 90°$ were calculated by varying N. The results for $N\Theta_{L_{S2}} = N\Theta_{L_{S1}} = 50°, 60°$, and $70°$ are listed in Tables IV and V and plotted in Fig. 12. The characteristic impedances of $Z_{L_{S2}}$ and $Z_{L_{S1}}$ in Fig. 12 are proportional to the electrical lengths of $N\Theta_{L_{S2}}$ or $N\Theta_{L_{S1}}$ and have the maximum value of 180 Ω when $N\Theta_{L_{S2}} = N\Theta_{L_{S1}} = 90°$. With N

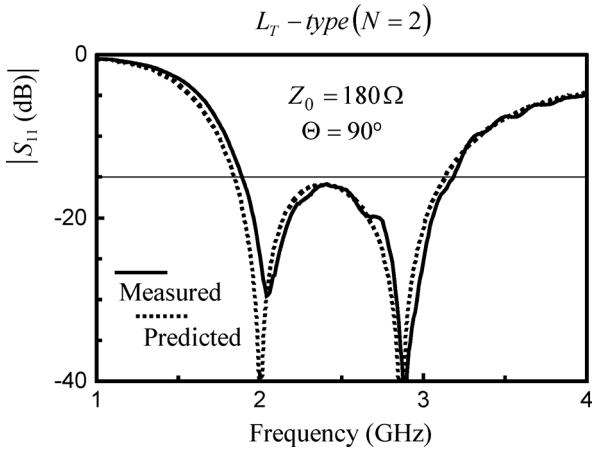

Fig. 11. Results measured and predicted are compared.

TABLE IV
DESIGN DATA OF L_{S2}- AND L_{S1}-TYPES FOR $N\Theta_{L_{S2}} = N\Theta_{L_{S1}} = 50°$ AND 70°, WHEN THE ORIGINAL TRANSMISSION-LINE SECTION HAVING $Z_0 = 180\ \Omega$ AND $\Theta = 90°$

	$N\Theta_{L_{S2}} = N\Theta_{L_{S1}} = 50°$		$N\Theta_{L_{S2}} = N\Theta_{L_{S1}} = 70°$	
N	$Z_{L_{S2}}$ (Ω)	$Z_{L_{S1}}$ (Ω)	$Z_{L_{S2}}$ (Ω)	$Z_{L_{S1}}$ (Ω)
$N=1$	137.89	83.94	169.15	126.04
$N=2$	107.58	96.34	146.01	137.02
$N=3$	103.25	98.40	142.59	138.71
$N=4$	101.81	99.11	141.44	139.28
$N=5$	101.15	99.43	140.92	139.54

TABLE V
DESIGN DATA OF L_{S2}- AND L_{S1}-TYPES FOR $N\Theta_{L_{S2}} = N\Theta_{L_{S1}} = 60°$, WHEN THE ORIGINAL TRANSMISSION-LINE SECTION HAVING $Z_0 = 180\ \Omega$ AND $\Theta = 90°$ AT 1 GHz

	$N\Theta_{L_{S2}} = N\Theta_{L_{S1}} = 60°$			
N	$Z_{L_{S2}}$ (Ω)	$Z_{L_{S1}}$ (Ω)	L_{S2}(nH)	L_{S1}(nH)
$N=1$	155.88	103.92	14.32	19.09
$N=2$	127.28	116.44	6.44	11.78
$N=3$	123.13	118.45	4.22	8.12
$N=4$	121.74	119.14	3.15	6.16
$N=5$	121.11	119.45	2.51	4.95

growing, the two values of $Z_{L_{S2}}$ and $Z_{L_{S1}}$ become about the same.

If it is assumed that a characteristic impedance of 120 Ω is realized without any difficulty, all the cases of the L_{S1}-type are possible with $N\Theta_{L_{S1}} = 50°$, while only four cases are possible for the L_{S2}-type from the data in Fig. 12. With the data for $N\Theta_{L_{S1}} = N\Theta_{L_{S2}} = 60°$ in Table V, the L_{S1}- and L_{S2}-types were simulated, and the simulation results of $|S_{11}|$ are plotted in Fig. 13 where the design center frequency is 1 GHz. If a bandwidth is defined as a frequency region where return loss is greater than 15 dB, the bandwidth of L_{S1}- and L_{S2}-types for $N = 2$ is about 225%, that for $N = 3$ is about 280%, while those for $N = 4$ and 5 are about 420% and 450%, respectively. Even better, the resulting transmission-line sections are 60° long, which is shorter than the original 90° transmission-line section.

d) Measurements of L_{S1}-Type With $N = 2$: For the verification of L_{S1}-type, one with $Z_0 = 180\ \Omega$ and $\Theta = 90°$ was designed at a design center frequency of 700 MHz and fabricated on the same substrate. To make use of available inductors with 20 nH (Murata, LQW18AN20NG00), the electrical length of $N\Theta_{L_{S1}}$ in Fig. 6(d) was determined as 52.5° with $N = 2$. Its corresponding characteristic impedance of $Z_{L_{S1}}$ is then 101.325 Ω, which can be realized without any problem. The fabricated L_{S1}-type is displayed in Fig. 14(a), and the measured frequency responses of $|S_{11}|$ and $|S_{21}|$ are compared with the predicted ones in Fig. 14 where good agreement is shown with the predicted ones.

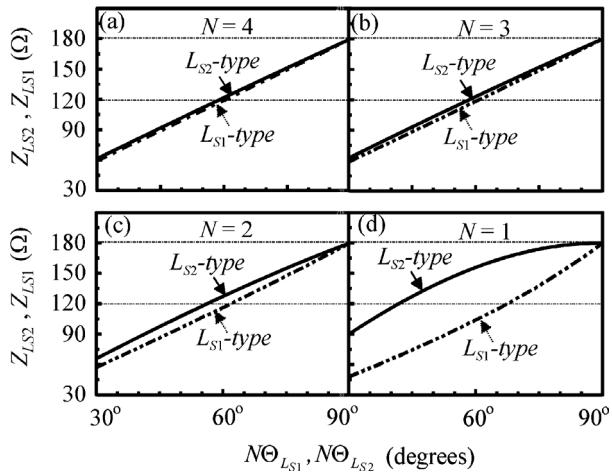

Fig. 12. Characteristic impedances of $Z_{L_{S2}}$ and $Z_{L_{S1}}$ for a transmission-line section with $Z_0 = 180\ \Omega$ and $\Theta = 90°$. (a) $N = 4$. (b)$N = 3$. (c) $N = 2$. (d) $N = 1$.

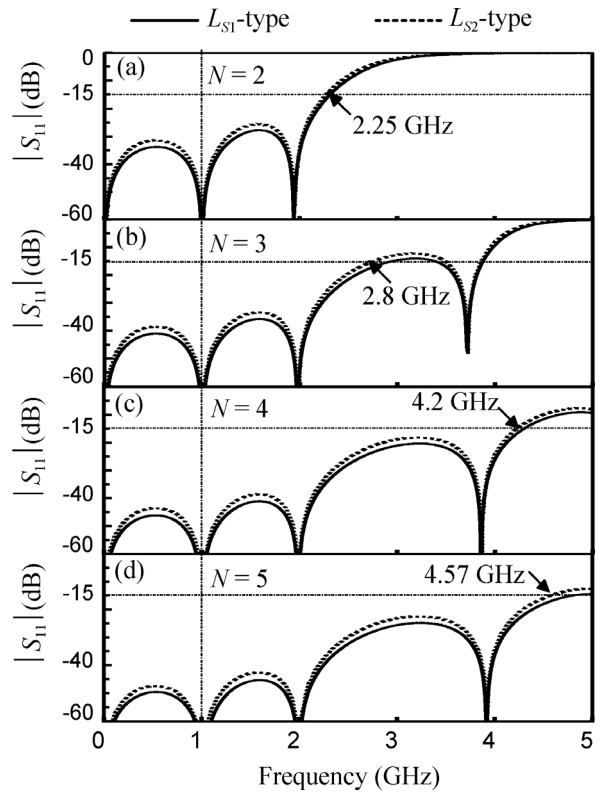

Fig. 13. Frequency responses of L_{S1}- and L_{S2}-types. (a) $N = 2$. (b) $N = 3$. (c) $N = 4$. (d) $N = 5$.

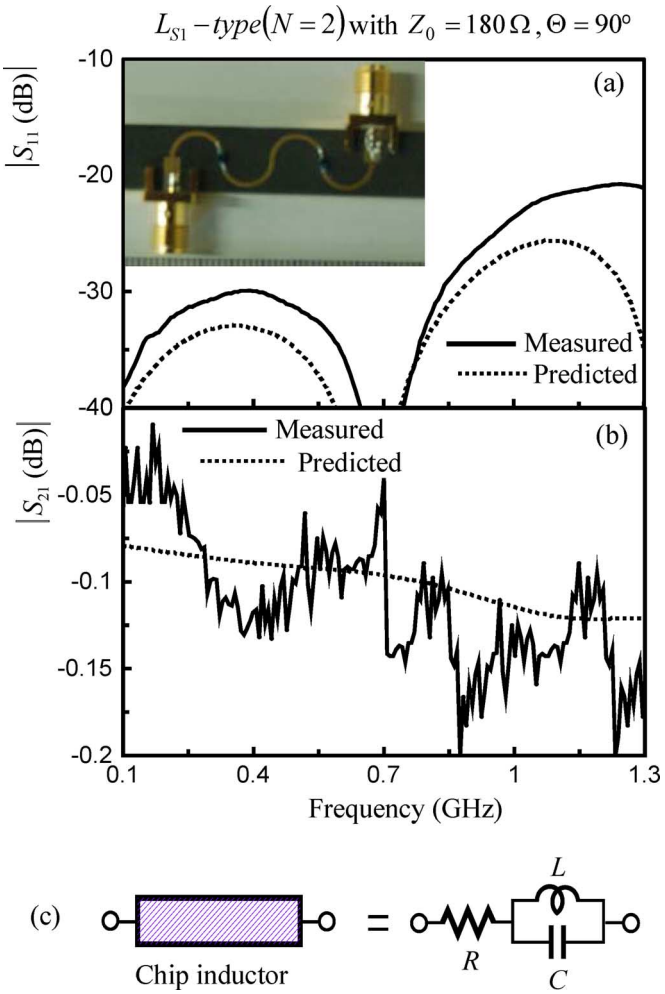

Fig. 14. Measured results of L_{S1}-type with $N = 2$. (a) S_{11}. (b) S_{12}. (c) Modeling of a lumped-element inductor.

The lumped-element inductor may be modeled as the circuit in Fig. 14(c) where a resistance of R is connected to a parallel resonator with a pure inductance of L and a pure capacitance of C. The pure inductance represents the value of the lumped-element inductor. The loss produced by the inductor is expressed as the resistance, and the capacitance of C is a parasitic element, which can determine the self resonance frequency of the lumped-element inductor. The self resonance frequency for the inductor is minimum of 5 GHz specified in the datasheet, from which the capacitance of C may be computed as 0.05 pF, and from the insertion loss, the resistance may also be extracted as 1.5 Ω.

D. Modified L_{S2}-Type (ML_{S2}-Type)

The characteristic impedance $Z_{L_{S2}}$ of the L_{S2}-type in Fig. 6(c) is definitely smaller than Z_0 of the original transmission-line section if $\Theta_{L_{S2}}$ is smaller than Θ with any N. Nevertheless, the structure of the L_{S2}-type itself is not suitable for the coupled-line ring hybrids due to the inductances of L_{S2} at both ends. The value of L_{S2} is inversely proportional to the operating frequencies, but proportional to the characteristic impedance of Z_0, as indicated in Fig. 5(d). If the operating

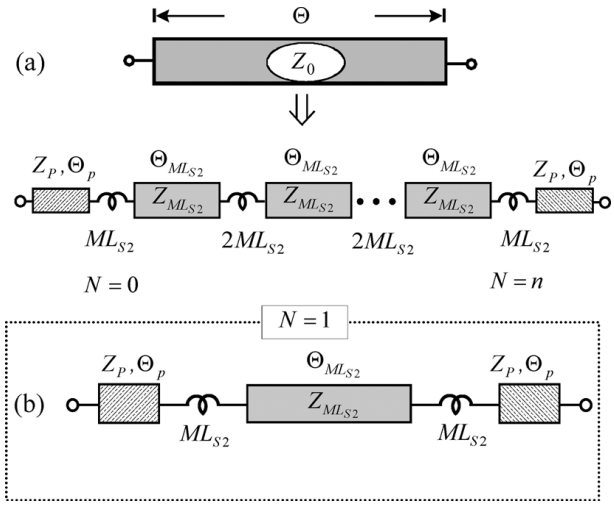

Fig. 15. ML_{S2}-type. (a) ML_{S2}-type with N. (b) ML_{S2}-type with $N = 1$.

frequencies are lower than 5 GHz, and the characteristic impedance of Z_0 is higher than 180 Ω, the inductance of L_{S2} cannot be realized with distributed elements and should be implemented with lumped-element inductors.

If it is desired to realize the inductance of the L_{S2}-type with a lumped element, for example, a 0402-sized chip inductor, half of the width of a 50-Ω transmission-line section on a substrate (RT/Duroid 5880, $\varepsilon_r = 2.2$, $H = 31$ mil) is wider than the length of the chip inductor. Therefore, it is almost impossible to form a Y-junction with the L_{S2}-type, i.e., to connect a third transmission-line section to make a port or to connect another transmission-line section, which results in incorrect operation of the L_{S2}-type.

To overcome the difficulty, modified L_{S2}-type (ML_{S2}-type), being equivalent to a transmission-line section with the characteristic impedance of Z_0 and arbitrary electrical length of Θ, is suggested in Fig. 15, where two identical transmission-line sections with the characteristic impedance of Z_P and the electrical length of Θ_P are connected to the inductances of the problem, as depicted in Fig. 15(a). The characteristic impedance of $Z_{L_{S2}}$, the electrical length of $\Theta_{L_{S2}}$, and the inductance of L_{S2} in the L_{S2}-type in Figs. 5(d) and 6(c) are changed to $Z_{ML_{S2}}$, $\Theta_{ML_{S2}}$, and ML_{S2}. The relations among $Z_{ML_{S2}}$, $\Theta_{ML_{S2}}$, and ML_{S2} are

$$Z_{ML_{S2}} = Z_Q \frac{\sin\Theta_{ML_{S2}}}{\sin\frac{\Theta_Q}{N}} \tag{9a}$$

$$\omega \cdot ML_{S2} = Z_Q \frac{\cos\Theta_{ML_{S2}} - cos\frac{\Theta_Q}{N}}{\sin\frac{\Theta_Q}{N}} \tag{9b}$$

where the design formulas for Z_Q and Θ_Q are shown in (9c) and (9d) at the bottom of the following page.

There are many solutions to $Z_{ML_{S2}}$, $\Theta_{ML_{S2}}$, and ML_{S2} by varying Z_P, Θ_P, and N. In the view of engineering perspective that the simplest is the most preferable, the ML_{S2}-type will be discussed intensively on $N = 1$, as displayed in Fig. 15(b). When $Z_P = 125$ Ω and $2\Theta_P + \Theta_{ML_{S2}} = 60°$ at 1 GHz are fixed for a 90° transmission-line section with $Z_0 = 180$ Ω, the design data are listed in Table VI, and frequency responses of

TABLE VI
DESIGN DATA OF THE ML_{S2}-TYPE WITH $N = 1$ FOR A TRANSMISSION-LINE SECTION HAVING $Z_0 = 180\ \Omega$ AND $\Theta = 90°$ AT 1 GHz

$\Theta_{ML_{S2}} + 2\Theta_P = 60°$, Z_P =125 Ω			
Θ_P	$Z_{ML_{S2}}$ (Ω)	$\Theta_{ML_{S2}}$	ML_{S2} (nH)
13°	119.19	34°	12.25
14°	116.31	32°	12.12
15°	113.34	30°	11.99
16°	110.25	28°	11.86
16.7°	108.01	26.6°	11.77
17°	107.03	26°	11.74

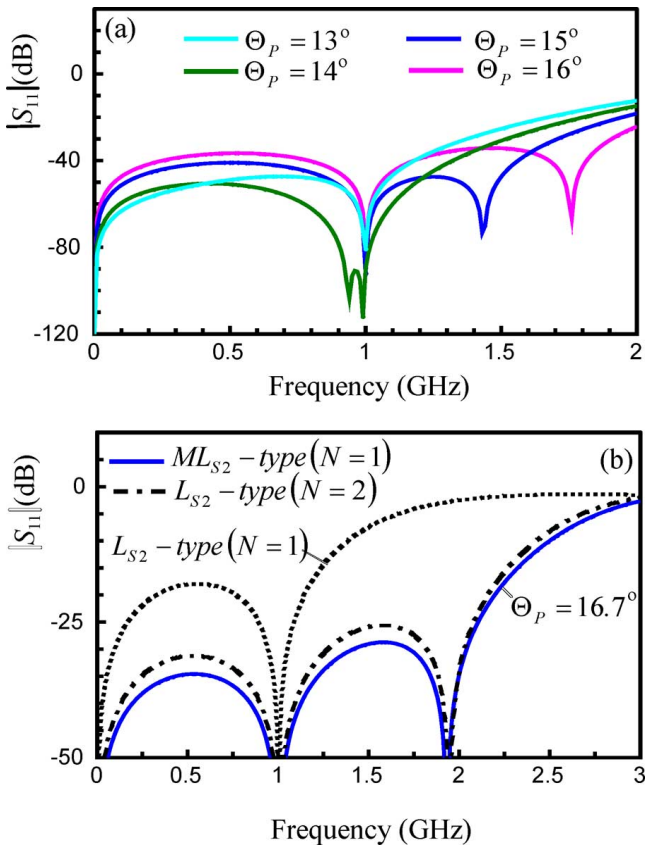

Fig. 16. Frequency responses. (a) ML_{S2}-types. (b) Comparisons between one ML_{S2}-type and L_{S2}-types with $N = 1$ and $N = 2$.

the several cases are plotted in Fig. 16(a). When $\Theta_P = 13°$ in Fig. 16(a), perfect matching occurs only at the design center frequency of 1 GHz. When $\Theta_P = 14°$, two perfect matching frequencies are possible; one is 1 GHz and another less than

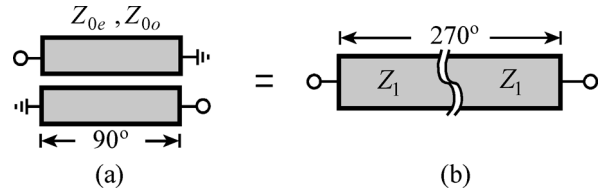

Fig. 17. (a) Set of coupled transmission-line sections. (b) Equivalent circuit.

1 GHz. When $\Theta_P = 15°$ or 16°, two poles exist for each case by which the bandwidths can be increased. This kind of frequency performance is not possible with the L_{S2}- and L_{S1}-types, as shown in Fig. 13.

The ML_{S2}-type with $\Theta_P = 16.7°$ is compared with L_{S2}-types with $N = 1$ and 2 in Fig. 16(b) where the frequency performance with the L_{S2}-type with $N = 1$ in [19] is the worst, even with the same number of inductances, while the ML_{S2}-type is better than the L_{S2}-type with $N = 2$, even with a less number of inductances. That much, the ML_{S2}-types have definite advantages over the L_{S2}-types, in terms of the substitutes of the high-impedance transmission line sections and better frequency performance.

IV. 90° COUPLED-LINE TRANSMISSION-LINE SECTIONS

A. Design Formulas

A set of coupled transmission-line sections with two short circuits in a diagonal direction and its equivalent circuit are depicted in Fig. 17 where the even- and odd-mode impedances are Z_{0e} and Z_{0o}, and the effective characteristic impedance of the equivalent transmission-line section in Fig. 17(b) is Z_1, as mentioned above in Fig. 1. As is well known, the electrical length of the equivalent transmission-line section is 270° if the coupled transmission-line sections are 90° long. In this case, the design formulas of the even- and odd-mode impedances Z_{0e} and Z_{0o} [3], [13], [16], [17] in Fig. 17(a) are

$$Z_{0e} = Z_1 \frac{10^{\frac{C_{\rm dB}}{20}}}{1-10^{\frac{C_{\rm dB}}{20}}} \tag{10a}$$

$$Z_{0o} = Z_1 \frac{10^{\frac{C_{\rm dB}}{20}}}{1+10^{\frac{C_{\rm dB}}{20}}} \tag{10b}$$

where $C_{\rm dB}$ is the coupling coefficient in dB.

B. Feasibility of Coupled Transmission-Line Sections

A pair of coupled transmission-line sections is a four-port circuit, and the circuit in Fig. 17(a) is obtained by placing short

$$Z_Q = Z_P \sqrt{\left(\frac{Z_0 \cot\frac{\Theta}{2} + Z_P \tan\Theta_P}{Z_P - Z_0 \cot\frac{\Theta}{2}\cdot\tan\Theta_P}\right)\left(\frac{Z_0 \tan\frac{\Theta}{2} - Z_P \tan\Theta_P}{Z_0 \tan\frac{\Theta}{2}\cdot\tan\Theta_P + Z_P}\right)} \tag{9c}$$

$$\tan\frac{\Theta_Q}{2} = \sqrt{\left(\frac{Z_P - Z_0 \cot\frac{\Theta}{2}\cdot\tan\Theta_P}{Z_P + Z_0 \tan\frac{\Theta}{2}\cdot\tan\Theta_P}\right)\left(\frac{Z_0 \tan\frac{\Theta}{2} - Z_P \tan\Theta_P}{Z_0 \cot\frac{\Theta}{2} + Z_P \tan\Theta_P}\right)} \tag{9d}$$

TABLE VII
PHYSICAL GAP SIZE OF THE COUPLED-LINE SECTIONS ON A SUBSTRATE (RT/DUROID 5870, $\varepsilon_r = 2.33$, $H = 0.787$ mm) WITH A FIXED COUPLING COEFFICIENT OF -10 dB AND A CENTER FREQUENCY OF 3 GHz

Z_1 (Ω)	(Z_{0e}, Z_{0o}) (Ω)	C_m (pF)	s (mm)
100 Ω	(46.2, 24.0)	46.27	0.039
200 Ω	(92.5, 48.1)	22.61	0.200
250 Ω	(115.6, 60.1)	17.91	0.272
300 Ω	(138.7, 72.1)	14.82	0.326
350 Ω	(161.9, 84.1)	12.61	0.365

circuits on two diagonal terminals. Since a set of the coupled transmission-line sections with an appropriate combination of short and open terminations produces special performance that a single transmission section is unable to provide, the usage of the coupled transmission-line sections is indispensable. The problem is, however, the feasibility of the even- and odd-mode impedances required. To realize a set of coupled transmission-line sections, the width of each transmission-line section and the gap size between two coupled transmission-line sections should be realizable. The width is related mainly with the even-mode impedance and the gap size with the mutual capacitance. To see the feasibility of the coupled transmission-line sections in Fig. 17(a), the relation between the mutual capacitance and the gap distance is investigated further.

The mutual capacitance C_m of a set of coupled transmission-line sections is expressed as

$$C_m = \frac{\sqrt{\mu\epsilon_{\text{eff}}}}{2}\left(\frac{1}{Z_{0o}} - \frac{1}{Z_{0e}}\right) \tag{11}$$

where $C_m = C_{12}$ in [23], and ϵ_{eff} and μ are effective permittivity and permeability of a substrate. The relation between the characteristic impedance of Z_1 in (10) of the coupled transmission-line sections and the mutual capacitance is

$$C_m = \frac{\sqrt{\mu\epsilon_{\text{eff}}}}{Z_1}. \tag{12}$$

Equation (12) expresses that the mutual capacitance C_m is inversely proportional to the characteristic impedance Z_1 of the coupled transmission-line sections. Due to this property, the easier fabrication is possible with the higher characteristic impedance of the coupled transmission-line sections. In the case of a substrate (RT/Duroid 5870, $\varepsilon_r = 2.33$, $H = 0.787$ mm) for an operating center frequency of 3 GHz, the mutual capacitance and the gap size are calculated (Table VII), and the results are plotted in Fig. 18. For the calculations, ADS (LineCalc) was used, and the coupling coefficient was fixed at -10 dB. For the characteristic impedance of $Z_1 = 100\ \Omega$, the even- and odd-mode impedances are 46.2 and 24.0 Ω, while the effective even- and odd-mode dielectric constants are 2.11 and 1.74. The mutual capacitance C_m is therefore 46.27 pF, as in Table VII. In this case, the required gap size is $s = 0.039$ mm, which is relatively difficult to fabricate in a planar structure of microstrip lines with a standard printed circuit board (PCB) technology. On the other hand, for $Z_1 = 250\ \Omega$, the effective even- and odd-mode dielectric constants are 1.94 and 1.67,

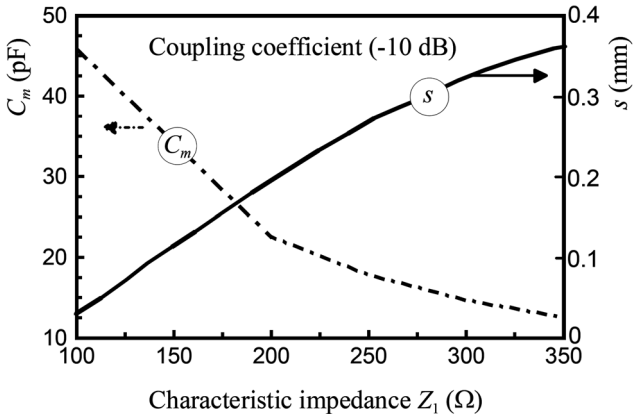

Fig. 18. Relation between mutual capacitance, gap size, and characteristic impedance of the coupled transmission-line sections.

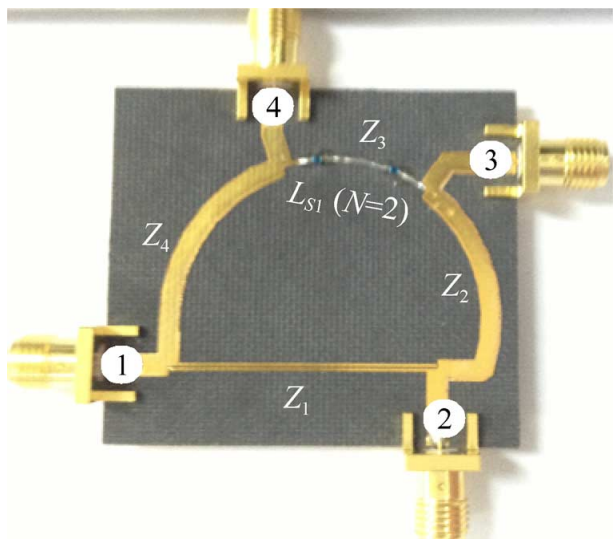

Fig. 19. Photograph of a fabricated ring hybrid with $P_{\text{dB}} = 13$ dB.

and therefore, $C_m = 17.91$ pF. The physical gap size becomes 0.27 mm, which is easier for the fabrication. In this way, the mutual capacitance is inversely proportional to the characteristic impedances of the coupled transmission-line sections with the fixed coupling coefficient. Thus, if the characteristic impedance of the coupled transmission-line sections becomes higher, it is easier to realize in terms of gap distance.

V. COUPLED-LINE RING HYBRIDS

To verify the suggested theory, two different coupled-line ring hybrids with the power-division ratios of 13 and 11 dB were fabricated on a substrate (RT/Duroid 5880, $\varepsilon_r = 2.2$, $H = 30$ mil).

A. $P_{\text{dB}} = 13$ dB

To implement a coupled-line ring hybrid, a design center frequency of 2 GHz was determined. The power-division ratio of P_{dB} was chosen as 13 dB, under the assumption of equal termination impedances of 50 Ω. In this case, $Z_1 = Z_3 = 228.9\ \Omega$ and $Z_2 = Z_4 = 51.2\ \Omega$, as calculated in Table II. To realize the characteristic impedance of 228.9 Ω, the coupling coefficient of the coupled transmission-line sections was chosen as -8.5 dB,

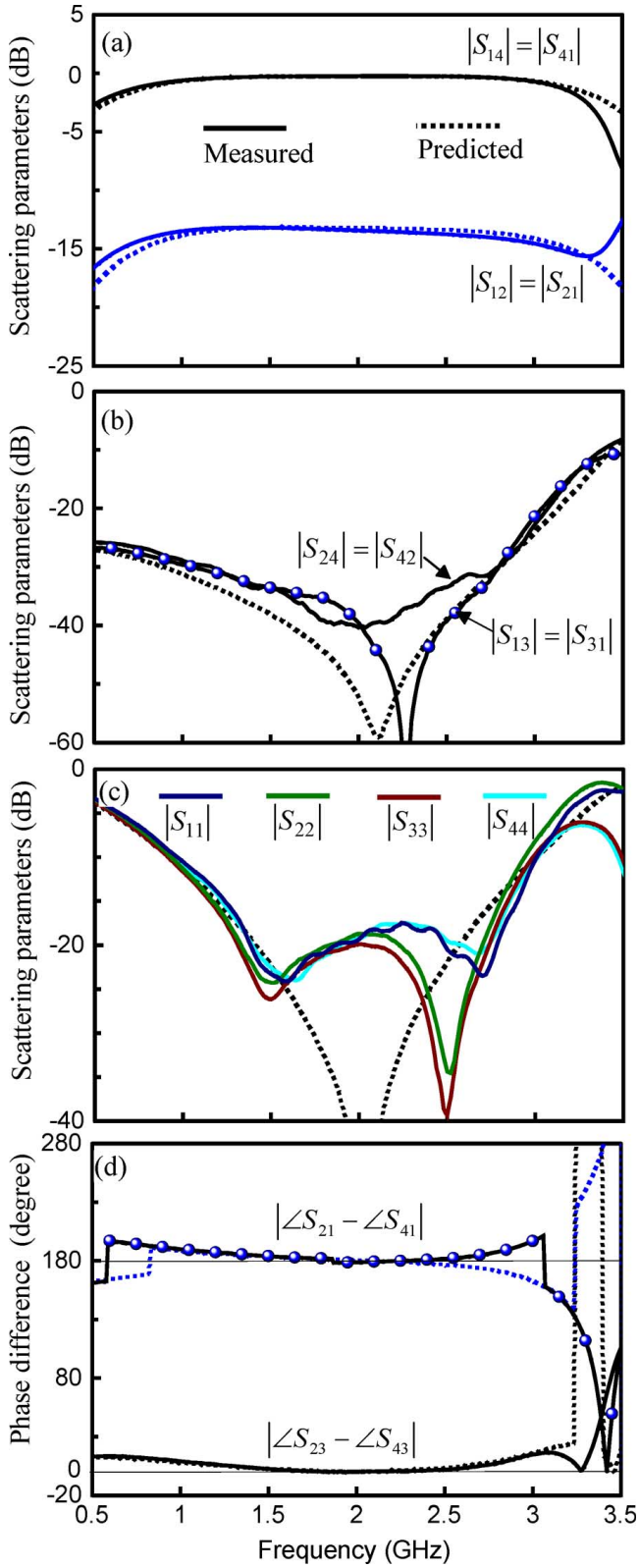

Fig. 20. Measured results with $P_{\rm dB} = 13$ dB. (a) Power divisions. (b) Isolations. (c) Matching. (d) Phase responses.

and the L_{S1}-type with $N = 2$ in Fig. 6(d) was employed for the single transmission-line section.

The corresponding Z_{0e} and Z_{0o} are 137.8 and 62.53 Ω for the coupled transmission-line sections, and the physical line

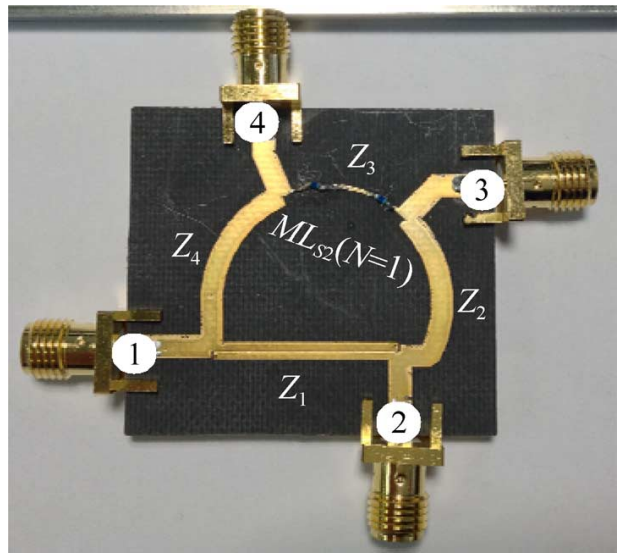

Fig. 21. Photograph of a fabricated ring hybrid with $P_{\rm dB} = 11$ dB.

width w and gap size s are $w = 0.319$ mm and $s = 0.176$ mm on the substrate. For the single transmission-line section with the characteristic impedance of $Z_3 = 228.9$ Ω in Fig. 1, to make use of available inductors with 9.1 nH (Murata, LQW15Aseries), the electrical length of $\Theta_{L_{S1}}$ in Fig. 6(d) is calculated as 25.29°, leading to $Z_{L_{S1}} = 123.98$ Ω. The fabricated ring hybrid is displayed in Fig. 19, and the measured results are in Fig. 20 where solid and dotted lines are the measured and predicted results.

The power-division responses are in Fig. 20(a), isolations in Fig. 20(b), matching responses in Fig. 20(c), and phase responses in Fig. 20(d). Since the ring hybrid in Fig. 19 was designed for the power-division ratio of 13 dB, or $20\log(d_2/d_1) = 13$, the scattering parameter of S_{21} is calculated as $10\log\{d_1^2/(d_1^2 + d_2^2)\}$, i.e., −13.21 dB. Due to the difference of 13 dB between S_{21} and S_{41}, the scattering parameter of S_{41} is −0.21 dB. The measured S_{21} and S_{41} are −13.732 and −0.245 dB at 2 GHz in Fig. 20(a), and the measured power-division ratio is 13.487 dB. In Fig. 20(b), the isolations of S_{31} and S_{24} are greater than 40 dB at 2 GHz and greater than 15 dB from 0 to 3.2 GHz. Since the simulated matching results at all ports have about the same responses, they are expressed with only a single dotted line in Fig. 20(c) where the measured return losses at all ports are greater than 20 dB at the design center frequency of 2 GHz, and the frequency bandwidth with 15-dB return loss is 1.15–2.9 GHz. The fact of the desirable isolations in Fig. 20(b) indicates that good in-phase and out-of-phase responses are possible. In Fig. 20(d) of the phase responses, the measured $|\angle S_{21} - \angle S_{41}|$ and $|\angle S_{23} - \angle S_{43}|$ at 2 GHz are obtained as 178.9° and 0.244°. The measured results are in good agreement with the predicted ones.

B. $P_{\rm dB} = 11$ dB

A coupled-line ring hybrid with $P_{\rm dB} = 11$ dB was fabricated on the same substrate, and the design center frequency

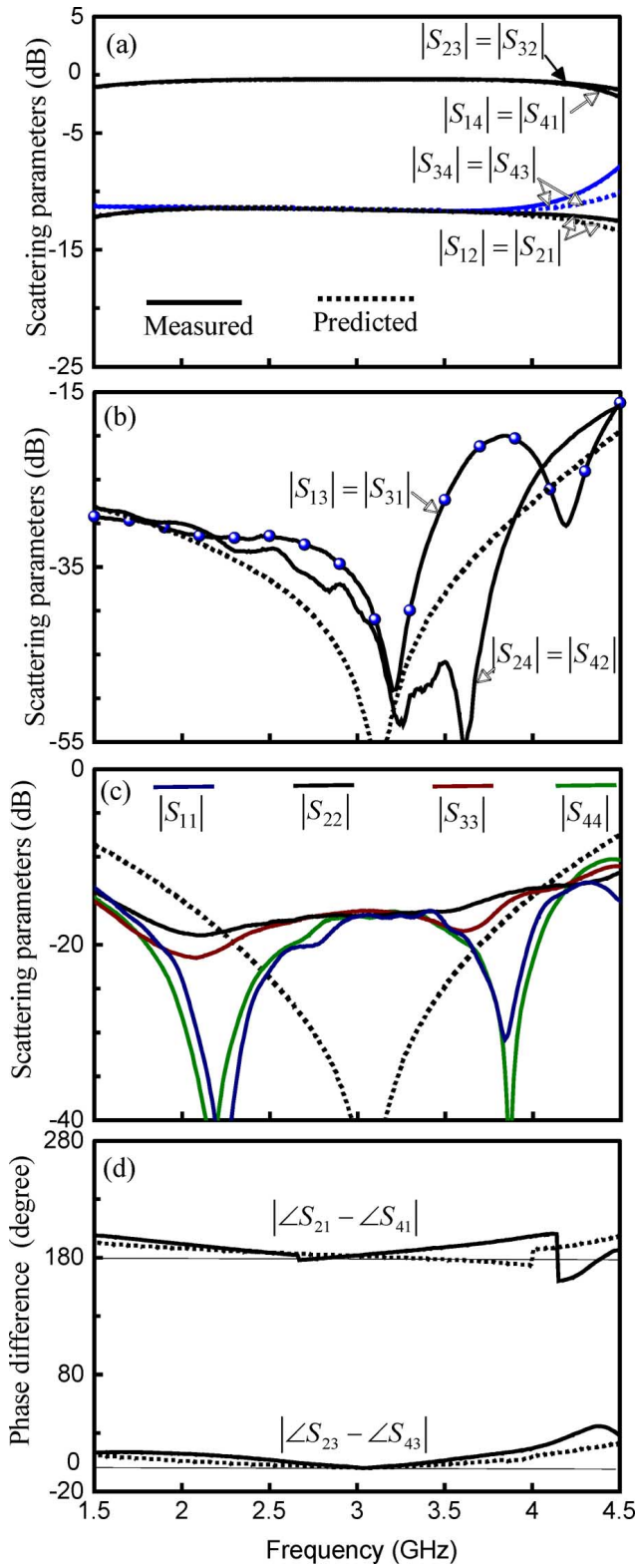

Fig. 22. Measured results with $P_{\mathrm{dB}} = 11$ dB. (a) Power divisions. (b) Isolations. (c) Matching. (d) Phase responses.

was chosen as 3 GHz. In this case, if all the termination impedances are assumed to be 50 Ω, $Z_1 = Z_3 = 184.32\ \Omega$ and $Z_2 = Z_4 = 51.95\ \Omega$, as calculated in Table II. To realize the characteristic impedance of 184.32 Ω for the single transmission-line section, the ML_{S2}-type with $N = 1$ in Fig. 15(b) was employed.

To make use of available inductors of 4.1 nH at 3 GHz, Z_P and Θ_P in Fig. 15(b) were predetermined as 125 Ω and 14.3°. $Z_{ML_{S2}} = 119.1\ \Omega$ and $\Theta_{ML_{S2}} = 31.4°$ were then calculated. For the coupled transmission-line sections, the coupling coefficient was chosen as -8 dB and its corresponding Z_{0e} and Z_{0o} are 121.9 and 52.48 Ω. The fabricated ring hybrid is in Fig. 21 where the ML_{S2}-type with $N = 1$ is indicated.

The measured and predicted results are compared in Fig. 22 where the measured power-division ratio is 11.26 dB in Fig. 22(a), the measured isolations are more than 15 dB in a frequency range of 1.5–4.5 GHz in Fig. 22(b), and return losses at all ports are more than 18 dB in a frequency range of 1.5–3.5 GHz in Fig. 22(c). The phase differences of $|\angle S_{21} - \angle S_{41}|$ are measured as $180° \pm 5°$ in the frequency range of 2.45–3.26 GHz, and those of $|\angle S_{23} - \angle S_{43}|$ are tested as $\pm 5°$ in 2.62–3.42 GHz in Fig. 22(d). The measured results, in general, agree with the predicted ones, given fabrication errors.

VI. Conclusion

In this paper, a wideband coupled-line ring hybrid has been suggested for high power-division ratios. For this, a 90° single transmission-line section and a set of 90° coupled transmission-line sections with high characteristic impedances are indispensible. To make the high values of characteristic impedances feasible for the single transmission-line sections, four types (L_{Π}-, L_T-, L_{S2}-, and L_{S1}-types) of equivalent circuits have been discussed, and an integer N has been introduced for wideband characteristics and design flexibilities. Even though all the characteristic impedances of the transmission-line sections in the four types are lower than that of the original transmission-line section, the L_{S2}-type cannot be utilized for the coupled-line ring hybrids with high power-division ratios. Therefore, the ML_{S2}-types were suggested, and ML_{S2}-types with $N = 1$ were intensively discussed.

Since the high-impedance transmission-line sections for both single and coupled transmission-line sections are needed for various applications including the ring hybrids demonstrated in this paper, many other applications are expected in microwave circuits.

References

[1] H.-R. Ahn, I.-S. Chang, and S. Yun, "Miniaturized 3-dB ring hybrid terminated by arbitrary impedances," *IEEE Trans. Microw. Theory Techn.*, vol. 42, no. 12, pp. 2216–2221, Dec. 1994.

[2] H.-R. Ahn, I. Wolff, and I.-S. Chang, "Arbitrary termination impedances, arbitrary power division, and small-sized ring hybrids," *IEEE Trans. Microw. Theory Techn.*, vol. 45, no. 12, pp. 2241–2247, Dec. 1997.

[3] H.-R. Ahn and B. Kim, "Small wideband coupled-line ring hybrids with no restriction on coupling power," *IEEE Trans. Microw. Theory Techn.*, vol. 57, no. 7, pp. 1806–1817, Jul. 2009.

[4] H.-R. Ahn, *Asymmetric Passive Components in Microwave Integrated Circuits*. New York, NY, USA: Wiley, 2006, pp. 56–121, P. 51.

[5] C. Y. Pon, "Hybrid-ring directional coupler for arbitrary power divisions," *IRE Trans. Microw. Theory Techn.*, vol. MTT-9, no. 6, pp. 529–535, Jun. 1961.

[6] A. K. Agrawal and G. F. Mikucki, "A printed-circuit hybrid-ring directional coupler for arbitrary power divisions," *IEEE Trans. Microw. Theory Techn.*, vol. MTT-34, no. 12, pp. 1401–1407, Dec. 1986.

[7] C.-L. Hsu, J.-T. Kuo, and C.-W. Chang, "Miniaturized dual-band hybrid couplers with arbitrary power division ratios," *IEEE Trans. Microw. Theory Techn.*, vol. 57, no. 1, pp. 149–156, Jan. 2009.

[8] M.-J. Park and B. Lee, "Design of ring couplers for arbitrary power division with 50 Ω lines," *IEEE Microw. Wireless Compon. Lett.*, vol. 21, no. 4, pp. 185–187, Apr. 2011.
[9] P.-L. Chi, "Miniaturized ring coupler with arbitrary power divisions based on the composite right/left-handed transmission lines," *IEEE Microw. Wireless Compon. Lett.*, vol. 22, no. 4, pp. 170–172, Apr. 2012.
[10] K.-K. M. Cheng and S. Yeung, "A novel rat-race coupler with tunable power dividing ratio, ideal port isolation, and return loss performance," *IEEE Trans. Microw. Theory Techn.*, vol. 61, no. 1, pp. 55–60, Jan. 2013.
[11] S. March, "A wideband stripline hybrid ring," *IEEE Trans. Microw. Theory Techn.*, vol. MTT-16, no. 6, pp. 361–362, Jun. 1968.
[12] H.-R. Ahn and I. Wolff, "Asymmetric ring hybrid phase-shifters and attenuators," *IEEE Trans. Microw. Theory Techn.*, vol. 50, no. 4, pp. 1146–1155, Apr. 2002.
[13] H.-R. Ahn and B. Kim, "Equivalent transmission-line sections for very high impedances and their application to branch-line hybrids with very weak coupling power," *J. Korean Inst. Electromagn. Eng. Sci.*, vol. 9, no. 2, pp. 85–97, Jun. 2009.
[14] T. T. Mo, Q. Que, and C. H. Chan, "A broadband compact microstrip rat-race hybrid using a novel CPW inverter," *IEEE Trans. Microw. Theory Tech.*, vol. 55, no. 1, pp. 161–165, Jan. 2007.
[15] T. Wang and K. Wu, "Size-reduction and band-broadening design technique of uniplanar hyabrid ring coupler using phase inverter for M(H)MIC's," *IEEE Trans. Microw. Theory Techn.*, vol. 47, no. 2, pp. 198–206, Feb. 1999.
[16] H.-R. Ahn, J. Kim, and B. Kim, "Branch-line hybrids with −15 dB coupling power," in *Asia–Pacific Microw. Conf. Dig.*, Hong Kong, Dec. 2008, pp. 1–4.
[17] B. Li, X. Wu, and W. Wu, "A 10:1 unequal Wilkinson power divider using coupled lines with two shorts," *IEEE Microw. Wireless Compon. Lett.*, vol. 19, no. 12, pp. 789–791, Dec. 2009.
[18] J.-L. Li and B.-Z. Wang, "Novel design of Wilkinson power dividers with arbitrary power division ratios," *IEEE Trans. Ind. Electron.*, vol. 58, no. 6, pp. 2541–2546, Jun. 2011.
[19] K. Hettak, G. A. Morin, and M. G. Stubbs, "The integration of thin-film microstrip and coplanar technologies for reduced-size MMICs," *IEEE Trans. Microw. Theory Techn.*, vol. 53, no. 1, pp. 283–291, Jan. 2005.
[20] J.-S. Lim, C.-S. Kim, J.-S. Park, D. Ahn, and S. Nam, "Design of 10 dB 90° branch line coupler using microstrip line with defected ground structure," *Electron. Lett.*, vol. 36, no. 21, pp. 1784–1785, Oct. 2000.
[21] L. Chiu and Q. Xue, "A parallel-strip ring power divider with high isolation and arbitrary power-dividing ratio," *IEEE Trans. Microw. Theory Techn.*, vol. 55, no. 11, pp. 2419–2426, Nov. 2007.
[22] S. Sun and L. Zhu, "Stopband-enhanced and size-miniaturized low-pass filters using high-impedance property of offset finite-ground microstrip line," *IEEE Trans. Microw. Theory Techn.*, vol. 53, no. 9, pp. 2844–2850, Sep. 2005.
[23] H.-R. Ahn and T. Itoh, "Impedance-transforming symmetric and asymmetric DC blocks," *IEEE Trans. Microw. Theory Techn.*, vol. 58, no. 9, pp. 2463–2474, Sep. 2010.

Hee-Ran Ahn (S'90–M'95–SM'99) received the B.S., M.S., and Ph.D. degrees in electronic engineering from Sogang University, Seoul, Korea, in 1988, 1990, and 1994, respectively.

Since April 2011, she has been with the School of Electrical Engineering and Computer Science, Seoul National University, Seoul Korea. From August 2009 to December 2010, she was with the Department of Electrical Engineering, University of California at Los Angeles, Los Angeles, CA, USA. From July 2005 to August 2009, she was with the Department of Electronics and Electrical Engineering, Pohang University of Science and Technology, Pohang, Korea. From 2003 to 2005, she was with the Department of Electrical Engineering and Computer Science, Korea Advanced Institute of Science and Technology, Daejeon, Korea. From 1996 to 2002, she was with the Department of Electrical Engineering, Duisburg–Essen University, Duisburg, Germany, where she was involved with the Habilitation dealing with asymmetric passive components in microwave circuits. She authored *Asymmetric Passive Component in Microwave Integrated Circuits* (Wiley, 2006). Her interests include high-frequency and microwave circuit designs and biomedical applications using microwave theory and techniques.

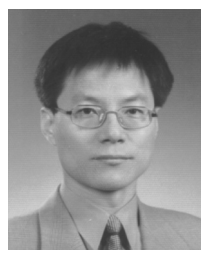

Sangwook Nam (S'87–M'88–SM'11) received the B.S. degree from Seoul National University, Seoul, Korea, in 1981, the M.S. degree from the Korea Advanced Institute of Science and Technology (KAIST), Seoul, Korea, in 1983, and the Ph.D. degree from The University of Texas at Austin, Austin, TX, USA, in 1989, all in electrical engineering.

From 1983 to 1986, he was a Researcher with the Gold Star Central Research Laboratory, Seoul, Korea. Since 1990, he has been a Professor with the School of Electrical Engineering and Computer Science, Seoul National University. His research interests include analysis/design of electromagnetic (EM) structures, antennas, and microwave active/passive circuits.